Thrust Control of the Permanent Magnet Linear Synchronous Motor with Multi-Frequency Resonant Controllers

Jia ZENG, Ghislain REMY, Philippe DEGOBERT, Pierre-Jean BARRE[1]
Laboratoire d'Electrotechnique et d'Electronique de Puissance de Lille (L2EP)
ENSAM, 8 Boulevard Louis XIV, 59046 Lille Cedex, France
URL: http://www.univ-lille1.fr/l2ep/
Tel: (+33) 3.20.62.22.29 Fax: (+33) 3.20.62.27.50
E-mail: Philippe.DEGOBERT@lille.ensam.fr

Keywords

Permanent Magnet Linear Synchronous Motor (PMLSM), resonant Controller, stationary frame control, thrust ripple, thrust control.

Abstract

Thrust control of the Permanent Magnet Linear Synchronous Motor (PMLSM) depends on the knowledge of the back electromotive force (EMF). To deal with a non-sinusoidal back EMF, the multiple reference frame theory can be applied, but it requires too much calculation. Thus, this paper proposes a simpler solution by using the multi-frequency resonant controllers in the stationary reference frame. With adaptive coefficients according to the input current frequency, the resonant controller can perfectly regulate the AC input current with variable frequency. To reduce the thrust ripple, an algorithm of generating the reference currents from the reference thrust is suggested to compensate for the non-sinusoidal back EMF. The simulated and experimental results demonstrate the efficiency of the proposed approach.

1 Introduction

With universally recognized advantages, the linear motors have been widely used in the transport and industrial fields. The field-oriented control with simple PI controllers in synchronous *d-q* reference frame has been applied to the Permanent Magnet Linear Synchronous Motor (PMLSM) and gave quite satisfactory performances [1]. However, it was assumed that the back EMF of the PMLSM is sinusoidal, and furthermore, the effects of stator inductance saliency have not been taken into account. Both of these neglected aspects will produce thrust ripple, especially the non-sinusoidal back EMF. In this condition, to achieve high-performance motion control and get smooth thrust force, non-sinusoidal currents need to be injected into the PMLSM [2]-[5].

The hysteresis controller can approximate the desired current waveforms [6] [7]. However, its major drawbacks lie in variable switching frequency and heavy interference among the phases in case of three-phase systems with isolated neutral. Furthermore, the tracking errors introduce undesired current harmonics that not only result in loss of optimal efficiency, but also in increased thrust ripple.

[1] J. ZENG, G. Remy, Ph. Degobert P. J. Barre, work in the research team of "Commande et Entraînement de Machines-Outils à DYNamique Elevée" (CEMODYNE), which is within the Laboratoire d'Electrotechnique et d'Electronique de Puissance de Lille (L2EP), ENSAM, 8 Bd Louis XIV, 59046 Lille Cedex, France, Tel: +33 3 20 62 22 46, Fax: +33 3 20 62 27 59 (e-mail: barre@lille.ensam.fr). This team is constituted of teachers - researchers of the L2EP, but also the LAIL and the LML.

The Multiple Reference Frame (MRF) theory has been applied to the control of the Permanent Magnet Synchronous Motor (PMSM) with non-sinusoidal back EFM, and satisfactory performances have been obtained [8] [9]. This theory was also suggested to control the PMLSM with salient inductances [10] and with non-sinusoidal back EMF [11]. A control scheme using Multiple Reference Frame Synchronous Estimator/Regulator (MRFSE/R), as shown in Fig. 1, is proposed in [11]. All the components of the harmonics of interest i_{dqk} are estimated from the measured currents i_{abc} by the MRFSR. The MRFSR can regulate these components so that i_{dqk} follows their respective references i^*_{dqk}. However, the major drawback of this approach lies in the large computational effort needed to establish the multiple reference frames: two coordinate transforms are required for every harmonic component. In even worse cases, to deal with the unbalanced condition, the number of reference frames should be doubled because the harmonics may appear both in positive and negative sequences. Furthermore, the control performances also depend on the accuracy of harmonic Fourier coefficients.

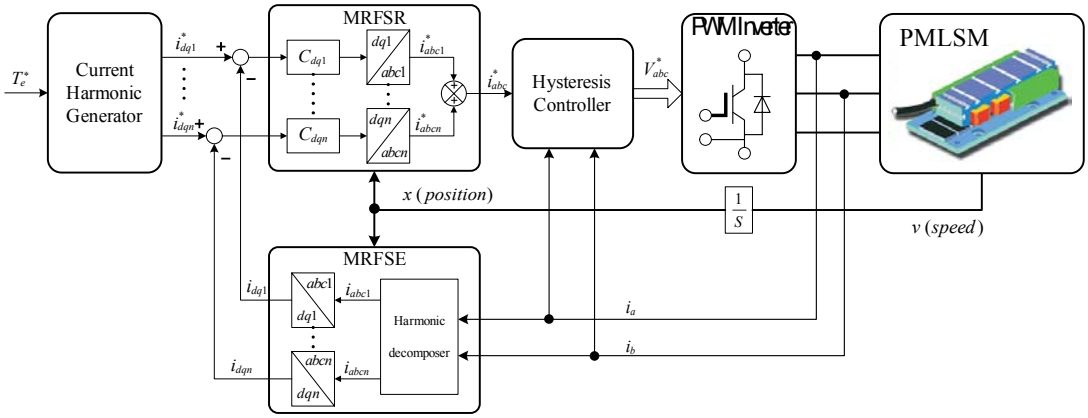

Fig. 1. Block diagram of thrust control of the PMLSM using Multiple Reference Frame Synchronous Estimator/Regulator.

In this paper, we will propose another approach based on the use of the resonance controller. This type of controller was first presented in [12] for the control of a PWM rectifier. Many research works have contributed to this subject in the last few years [13]-[17]. By associating an arbitrary number of resonant elements in series, the multi-frequency resonant controller can get infinite gains at the selected resonant frequencies in the open-loop system, thereby completely eliminating the steady-state control errors of the fundamental component as well as the harmonics components at the same resonant frequencies.

Usually, the feed of the PMLSM requires variation of the load current frequency. To guarantee the dynamic control performances, all coefficients of the resonant controller should be adjusted according to the input current frequencies. By this means, the regulated current can perfectly follow its reference after a short transition, even if the frequency of the reference current varies with time.

In this paper, after the modeling of a three-phase-three-line PMLSM with non-sinusoidal back EMF, a thrust control scheme is set up in the stationary $\alpha-\beta$ reference frame. To reduce the thrust ripple caused by the harmonics of the magnet flux, the reference currents deduced from the reference thrust are investigated and suggested by this paper. By using the multi-frequency resonant controllers, the load currents in the PMLSM can perfectly follow the proposed non-sinusoidal current references, and thereby, significantly reduce the thrust ripple of the PMLSM.

2 The PMLSM Model in the Stationary α - β Reference Frame

In this section, we set forth a machine model for a three-phase-three-line PMLSM with a non-sinusoidal back EMF. We assume that the PMLSM exhibits no effects of saturation or demagnetization and that the back EMF waveform is half-wave symmetric and thus has no even harmonics. Fig. 2 depicts the simplified schematic of a short primary iron core PMLSM. Mechanical position and speed of the primary are denoted by x and v, respectively. The electrical angle and angular speed, θ_e and ω, are defined as N_p times the corresponding mechanical quantities, where $N_p = \pi / \tau$ is the electrical position constant of the PMLSM (τ : step between two consecutive magnetic poles of secondary) [18].

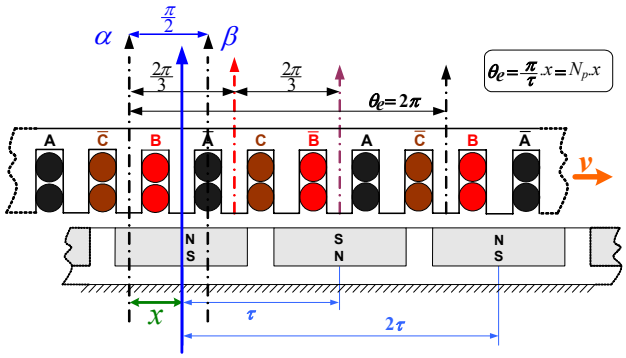

Fig. 2. Simplified schematic of the PMLSM.

The stator voltage equations may be expressed as:

$$[V_{abc}] = [R] \cdot [i_{abc}] + \frac{d[\phi_{abc}]}{dt} \quad . \tag{1}$$

where R denotes the stator resistances; V_{abc}, i_{abc} and ϕ_{abc} represent the voltage, current and flux linkage vectors, respectively.

Neglecting the inductance saliency (surface-mounted permanent magnet PMLSM), phenomena of longitudinal end-effects, and assuming that the back EMF is half wave symmetric, the stator flux linkage equations may be expressed as:

$$[\phi_{abc}] = [L_{abc}] \cdot [i_{abc}] + \hat{\phi}_f \cdot \sum_{n=1}^{\infty} \lambda_{2n-1} \begin{bmatrix} \cos[(2n-1)\theta_e] \\ \cos[(2n-1)(\theta_e - 2\pi/3)] \\ \cos[(2n-1)(\theta_e - 4\pi/3)] \end{bmatrix} . \tag{2}$$

L_{abc} is the stator inductance matrix and $\hat{\phi}_f$ denotes the maximum value of magnetic excitation flux per phase in a stationary *a-b-c* frame. The coefficients λ_{2n-1} represent the relative magnitude of the (2n-1)'th magnet flux harmonic. These coefficients are normalized by the fundamental component such as $K_1 = 1$.

The three-phase components in (1) can be transformed into equivalent orthogonal $\alpha\beta$ components through the $\alpha\beta - abc$ conservative transformation. The relations between the abc components and the $\alpha\beta$ components are given by:

$$[f_{abc}] = [T] \cdot [f_{\alpha\beta}] \quad \text{and} \quad [f_{\alpha\beta}] = [T^{-1}] \cdot [f_{abc}] \quad . \tag{4}$$

where

$$T=\begin{bmatrix}\sqrt{\frac{2}{3}} & 0\\ -\frac{1}{\sqrt{6}} & \frac{1}{\sqrt{2}}\\ -\frac{1}{\sqrt{6}} & -\frac{1}{\sqrt{2}}\end{bmatrix}\quad,\quad T^{-1}=\begin{bmatrix}\sqrt{\frac{2}{3}} & -\frac{1}{\sqrt{6}} & -\frac{1}{\sqrt{6}}\\ 0 & \frac{1}{\sqrt{2}} & -\frac{1}{\sqrt{2}}\end{bmatrix}. \tag{5}$$

Then, the stator voltage equations in the $\alpha-\beta$ reference frame can be expressed by:

$$\left[V_{\alpha\beta}\right]=\left[R\right]\cdot\left[i_{\alpha\beta}\right]+\left[L_{\alpha\beta}\right]\cdot\frac{d\left[i_{\alpha\beta}\right]}{dt}+N_p\cdot v\cdot\sqrt{\frac{3}{2}}\cdot\hat{\phi}_f\cdot\sum_{n=1}^{\infty}\left\{\left(2n-1\right)\cdot\lambda_{2n-1}\cdot\begin{bmatrix}K_\alpha^{2n-1}\cdot\sin\left[\left(2n-1\right)\theta_e\right]\\ K_\beta^{2n-1}\cdot\cos\left[\left(2n-1\right)\theta_e\right]\end{bmatrix}\right\}. \tag{6}$$

Where

$$\left[L_{\alpha\beta}\right]=\begin{bmatrix}L_\alpha & 0\\ 0 & L_\beta\end{bmatrix}. \tag{7}$$

$$K_\alpha^i=-\frac{2}{3}\left[1-\cos\left(\frac{2\pi}{3}\cdot i\right)\right],\qquad K_\beta^i=\left[\frac{2}{\sqrt{3}}\sin\left(\frac{2\pi}{3}\cdot i\right)\right]. \tag{8}$$

By using coenergy techniques and neglecting the cogging phenomena, the thrust generated by the PMLSM may be derived as:

$$T_e=\left[i_{\alpha\beta}\right]^t\cdot N_p\cdot\sqrt{\frac{3}{2}}\cdot\hat{\phi}_f\cdot\sum_{n=1}^{\infty}\left\{\left(2n-1\right)\cdot\lambda_{2n-1}\cdot\begin{bmatrix}K_\alpha^{2n-1}\cdot\sin\left[\left(2n-1\right)\theta_e\right]\\ K_\beta^{2n-1}\cdot\cos\left[\left(2n-1\right)\theta_e\right]\end{bmatrix}\right\}. \tag{9}$$

Furthermore, although the triple harmonics are non-zero quantities, they have no contributions to the overall thrust (since $K_\alpha^i, K_\beta^i\big|_{i=3k}=0$ with $\left\{k\in\mathbf{N}\right\}$). Thus, the thrust can be expressed by:

$$T_e=N_p\cdot\sqrt{\frac{3}{2}}\cdot\hat{\phi}_f\cdot\begin{bmatrix}i_\beta\left(\sum_{i=0}^{\infty}\left\{(6n+1)\lambda_{6n+1}\cdot\cos\left[(6n+1)\theta_e\right]\right\}-\sum_{i=0}^{\infty}\left\{(6n+5)\lambda_{6n+5}\cdot\cos\left[(6n+5)\theta_e\right]\right\}\right)\\ -i_\alpha\left(\sum_{i=0}^{\infty}\left\{(6n+1)\lambda_{6n+1}\cdot\sin\left[(6n+1)\theta_e\right]\right\}+\sum_{i=0}^{\infty}\left\{(6n+5)\lambda_{6n+5}\cdot\sin\left[(6n+5)\theta_e\right]\right\}\right)\end{bmatrix}. \tag{10}$$

3 Thrust Ripple Reduction Strategy

The studied PMLSM in this paper is an INDRAMAT prototype with a nominal power of 12 kW and a nominal linear speed of 185 m/min, other parameters are listed in TABLE I. The relative magnitudes of the magnet flux harmonics are identified through spectral analysis of the back EMF. Because the neutral of the motor is not accessible (three-phase-three-line), those of the triple harmonics can not be identified well and truly. However, since they have no contributions to the overall thrust force, as described in (10), we don't need these values in the thrust control.

TABLE I. SPECIFICATIONS OF THE STUDIED PMLSM

PMLSM parameters	Values	Parameters	Values
Stator inductance	$L_\alpha = L_\beta = 16.2\,[mH]$	Relative magnitude of the magnet flux harmonics	$\lambda_1 = 1$
Stator resistance	$R_s = 1.1\,[\Omega]$		λ_3 is unidentified
Max value of magnet flux per phase	$\hat{\phi}_f = 0.65\,[Wb]$		$\lambda_5 = -0.02667$
Pole Pitch	$\tau = 37.5\,[mm]$		$\lambda_7 = 0.0004234$
Electrical position constant	$N_p = 83.8\,[mm^{-1}]$		λ_9 is unidentified
Mass of mobile part	$M = 235\,[Kg]$		$\lambda_{11} = 0.0004589$

When neglecting the effects of magnet flux harmonics (supposing the back EFM to be sinusoidal), the reference currents, i_α^* and i_β^*, are sinusoidal and can be deduced from the reference thrust T_e^*, as expressed in (11).

$$\begin{cases} i_\alpha^* = \dfrac{-T_e^*}{N_p \cdot \sqrt{3/2} \cdot \hat{\phi}_f} \cdot \sin(\theta_e) \\ i_\beta^* = \dfrac{T_e^*}{N_p \cdot \sqrt{3/2} \cdot \hat{\phi}_f} \cdot \cos(\theta_e) \end{cases} . \tag{11}$$

By substituting these expressions for the currents i_α, i_β in (10), we notice that thrust ripples will be introduced by the nonzero magnet flux harmonics coefficients λ_i. Therefore, it is necessary to modify the reference currents to reduce these ripples. The thrust ripples caused by the 7th and 11th harmonics are very slight, 0.3% and 0.5% respectively, whereas that of the 5th harmonic should not be neglected (13.3%). In consideration of the control performance and reducing computation effort simultaneously, we only take the 5th harmonic into account in our control law. As a consequence, (10) can be simplified into:

$$T_e = N_p \cdot \sqrt{\frac{3}{2}} \cdot \hat{\phi}_f \cdot \left\{ i_\beta \left[\cos(\theta_e) - 5\lambda_5 \cdot \cos(5\theta_e) \right] - i_\alpha \left[\sin(\theta_e) + 5\lambda_5 \cdot \sin(5\theta_e) \right] \right\} . \tag{12}$$

And the reference currents, with which the thrust ripple can be completely eliminated from the generated thrust T_e in (12), can also be deduced from the reference thrust T_e^* and given by (13):

$$\begin{cases} i_\alpha^* = \dfrac{T_e^*}{N_p \cdot \sqrt{3/2} \cdot \hat{\phi}_f \cdot (1 - 25\lambda_5^2)} \cdot \left[-\sin(\theta_e) + 5\lambda_5 \cdot \sin(5\theta_e) \right] \\ i_\beta^* = \dfrac{T_e^*}{N_p \cdot \sqrt{3/2} \cdot \hat{\phi}_f \cdot (1 - 25\lambda_5^2)} \cdot \left[\cos(\theta_e) + 5\lambda_5 \cdot \cos(5\theta_e) \right] \end{cases} . \tag{13}$$

4 Multi-Frequency Resonant Controller

Resonant controller has been proved effective for AC current control in the stationary reference frame [12]-[17]. The multi-frequency resonant controller, which is used to regulate the non-sinusoidal signal, can be created by associating an arbitrary number of resonant elements in series. The aim is to get infinite gains at the selected resonant frequencies ω_i in the open-loop system, thereby allowing the steady-state control errors at the same frequencies to be completely eliminated. The transfer function of a controller with β resonant elements associated can be expressed by (14):

$$C(s)=\frac{\sum_{\alpha=0}^{2\beta} b_\alpha s^\alpha}{\prod_{i=1}^{\beta}\left(s^2+\omega_i^2\right)}, \qquad \{b_\alpha, \omega_i \in \mathbf{R}\} \quad . \tag{14}$$

Fig. 3 shows a current control system using a multi-frequency resonant controller. L and R denote, respectively, the inductance and resistance of the inductive load. The characteristic polynomial of closed-loop system is given by:

$$P(s)=\left(s-\frac{R}{L}\right)\cdot\prod_{i=1}^{\beta}\left(s^2+\omega_i^2\right)+\frac{1}{L}\cdot\sum_{\alpha=0}^{2\beta} b_\alpha s^\alpha \quad . \tag{15}$$

The coefficients of controller b_α can be determined by using the pole assignment technique – identifying the characteristic polynomial (14) by a criterion polynomial as shown in (16):

$$P_{GSM}(s)=(s+r)\prod_{i=1}^{\beta}\left[(s+r+j\Omega_i)(s+r-j\Omega_i)\right] \quad . \tag{16}$$
$$\{r, \Omega_i \in \mathbf{R};\ i \in \mathbf{N}\}$$

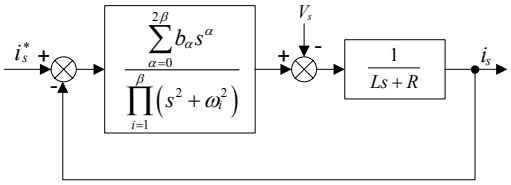

Fig. 3. AC current control system using multi-frequency resonant controller.

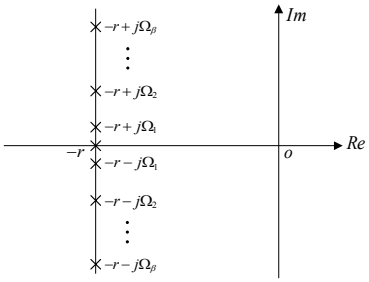

Fig. 4. Pole locations of the closed-loop system identified by proposed criterion polynomial.

By this means, all poles of the closed-loop system will be placed on a vertical line in the pole-zero map, as shown in Fig. 4. The imaginary parts are given by the values of the resonance frequencies Ω_i; the abscissa of this line is offered by r, which determines the dynamic response as well as the stability of the control system. Here, we choose $\Omega_i = \omega_i$ to control all system zeros around another vertical line, therefore minimiziing their influence on system stability.

Fig. 5 reports the magnitude and phase characteristics of the open-loop transfer functions $i_s(s)/i_s^*(s)$ of a current control system as described in Fig. 3, in which a 2-frequency resonant controller is used. We observe that large gains are produced at selected frequencies ($\omega_p, 5\omega_p$), which ensures that the steady-state errors for the input current harmonics of these frequencies can be completely eliminated. The bode diagram of the closed-loop transfer function (Fig. 6) presents a characteristic of unity gains (0dB) and zero phases at the selected frequencies, further confirming that the control system can perform zero steady-state error at these frequencies.

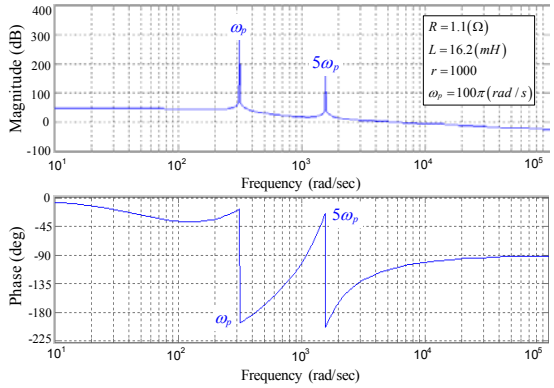

Fig. 5. Bode diagram of the open-loop transfer function of the inductive load current system using 2-frequency resonant controller.

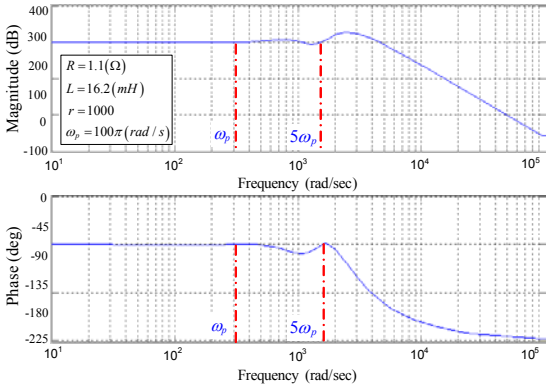

Fig. 6. Bode diagram of the closed-loop transfer function of the inductive load current system using 2-frequency resonant controller.

5 Thrust Control Scheme

The block diagram of a PMLSM thrust control system in the stationary $\alpha-\beta$ reference frame may be as shown in Fig. 7, where two multi-frequency resonant controllers are used. The $\alpha\beta$ axes reference currents, i_α^* and i_β^*, are generated by the reference current generator according to the reference thrust T_e^* and the position information of the PMLSM primary. The three-phase load currents are measured and transformed into $\alpha\beta$ axes, namely i_α and i_β, which are compared with i_α^* and i_β^*, then respectively regulated by a resonant controller. The speed of the primary is also measured and fed into the resonant controller. By this means, the coefficients of the controllers can be adjusted according to the input current frequency.

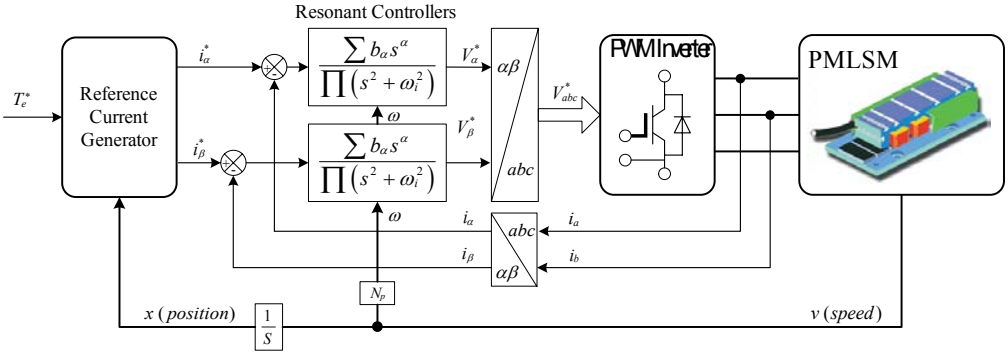

Fig. 7. Block diagram of thrust control of the PMLSM using multi-frequency resonant controllers.

6 Simulated and Experimental Results

After simulated investigation by a MATLAB/Simulink based model, the approach that is proposed in this paper has been experimentally validated using a laboratory test system (Fig. 8). The control scheme, as depicted in Fig. 7, is implemented in DS1005 card and drives a PMLSM prototype from INDRAMAT through an IGBT inverter. An incremental encoder is used to detect the primary speed. Since a suitable thrust dynamometer was not available, the generated thrust is estimated from the measured currents. All specifications of the test system are listed in TABLE I and TABLE II.

Fig. 9 depicts the system control performances obtained by simulation and experiment, where the sinusoidal reference currents of (11) are used and applied to the control system. The regulated currents follow their references perfectly, as shown in Fig. 9 (b) and (c). Nevertheless, we can observe that a ripple of about 15% of the average thrust presents in the estimated thrust. Here, the frequency of the

most important component of this thrust ripple is 6 times the current fundamental frequency, which is caused by the fundamental current interacting with the 5th harmonic of the magnet flux.

Fig. 10 shows the control performances while the proposed algorithm is applied – the reference currents are generated from the reference thrust T_e^* according to (13). As shown in Fig. 10 (b) and (c), due to the multi-frequency resonant controllers, the regulated currents can still perfectly follow their references, even if they are non-sinusoidal and with a frequency varying with time. From Fig. 10 (a), we can see that the thrust ripple of 6 times the current fundamental frequency that presents in Fig. 9(a) is completely eliminated. The thrust ripple caused by higher harmonics of the magnet flux is limited within 5% in experiment result. It is higher than that of in simulated result (within 1%), since the harmonics of the magnet flux higher than 11th has not been taken into account in simulation, furthermore, the noises in current and speed measurements may also increase the thrust ripple. Fig. 10 (d), (e) and (f) show the three-phase currents, linear speed and moved distance of the primary, respectively.

Fig. 8. Laboratory test system

TABLE II. SPECIFICATIONS OF TEST SYSTEM

Resonant controller	Selected frequencies	1st, 5th harmonics
	Stability margin	$r = 1000$
DC supply voltage		$V_{dc} = 570\,[V]$
Switching frequency of IGBT		$10\,[KHz]$

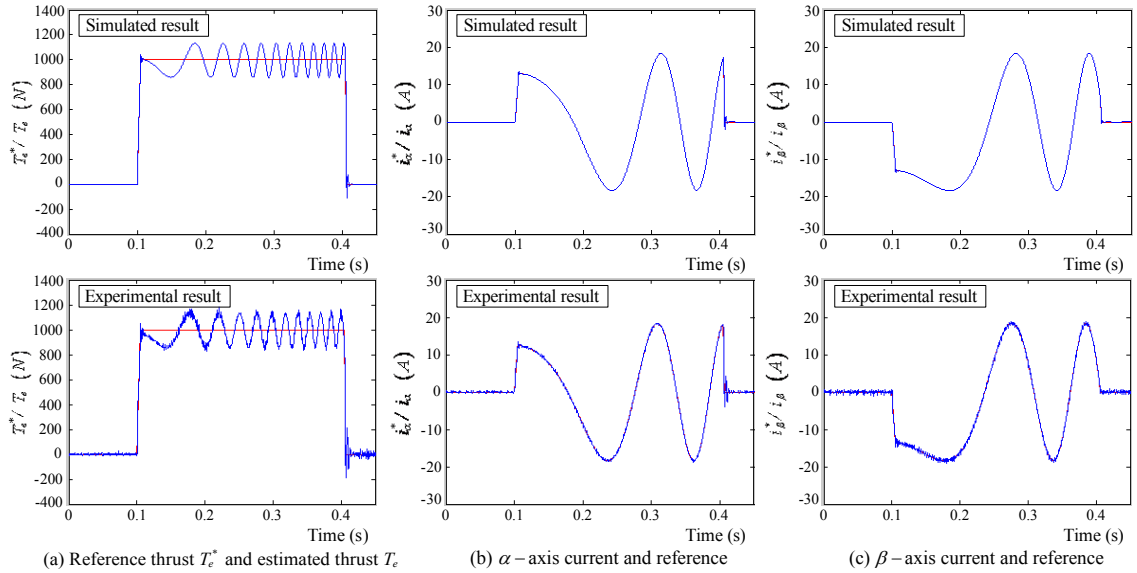

(a) Reference thrust T_e^* and estimated thrust T_e (b) α – axis current and reference (c) β – axis current and reference

Fig. 9. Simulated and experimental results with sinusoidal reference currents from (11).

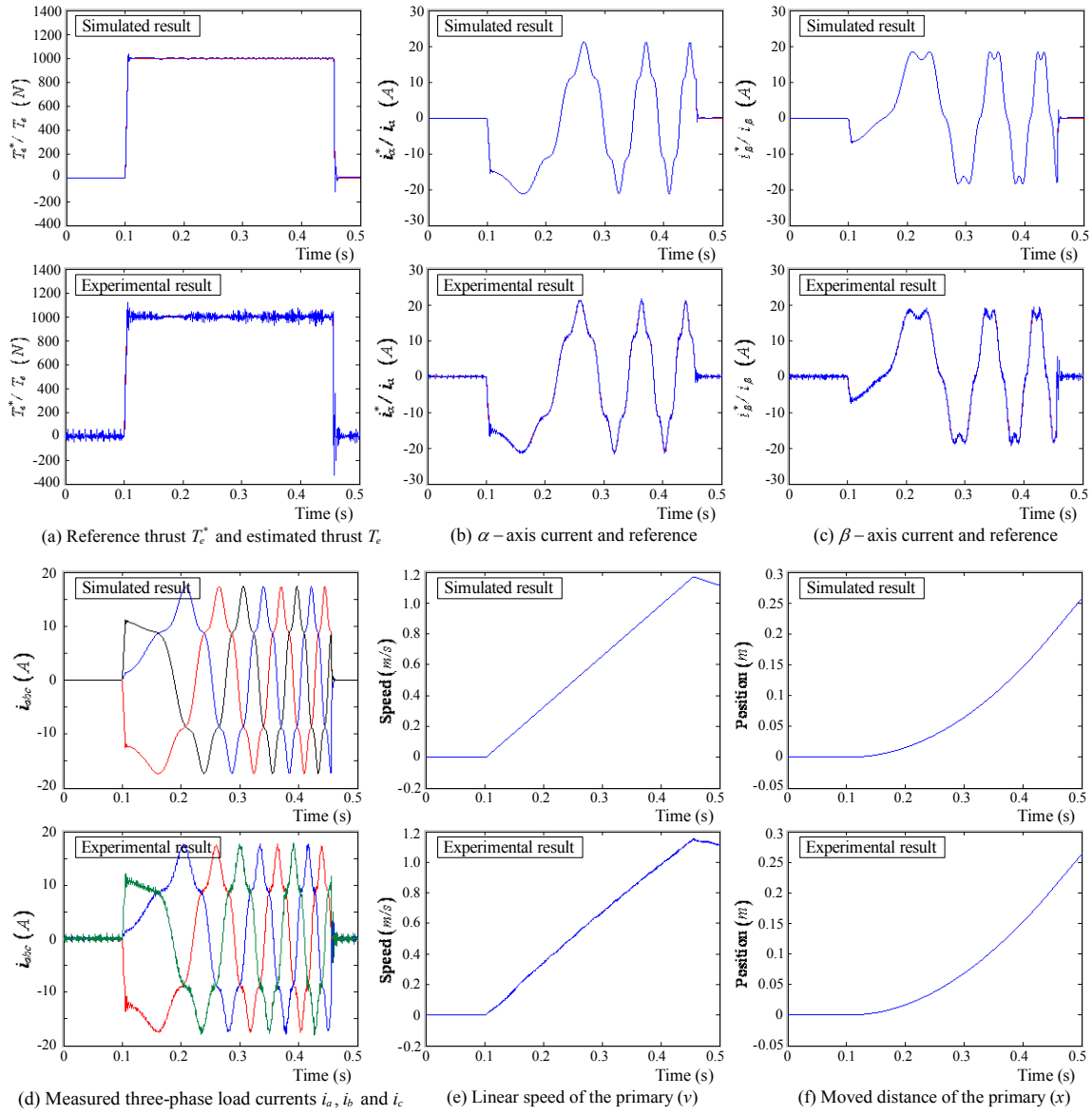

(a) Reference thrust T_e^* and estimated thrust T_e (b) $\alpha-$axis current and reference (c) $\beta-$axis current and reference

(d) Measured three-phase load currents i_a, i_b and i_c (e) Linear speed of the primary (v) (f) Moved distance of the primary (x)

Fig. 10. Simulated and experimental results with non-sinusoidal reference currents from (13).

7 Conclusions

This paper has presented a novel approach to improve the thrust control performance of a PMLSM with non-sinusoidal back EMF. First, an algorithm for generating the reference currents from the reference thrust is suggested to compensate for the non-sinusoidal EMF. Next, a multi-frequency resonant controller was proposed to ensure the tracking of the desired current waveforms. At last, a thrust control scheme of the PMLSM is set forth in the stationary $\alpha-\beta$ reference frame. The proposed approach has been proven efficient to reduce the thrust ripple of the PMLSM by simulated and experimental results.

8 Nomenclature

$V_{abc}, i_{abc}, \phi_{abc}$	Voltages, currents and flux in *abc* reference frame	x, v	Linear distance and velocity
$V_{\alpha\beta}, i_{\alpha\beta}, \phi_{\alpha\beta}$	Voltages, currents and flux in $\alpha\beta$ reference frame	θ_e, ω	Electrical angle and angular speed
R	Stator resistances	T_e, T_e^*	Thrust and reference thrust
L_{abc}	Stator inductances in *abc* reference frame	M	Mass of the primary of the PMLSM
L_α, L_β	Stator inductances in $\alpha\beta$ reference frame	N_p	Electrical position constant. $N_p = \pi/\tau$
$\hat{\phi}_f$	Maximum value of magnetic excitation flux per phase in *abc* reference frame	τ	Pole pitch: Step between two consecutive magnetic poles of secondary

References

1. J. Zeng, P.J. Barre, P. Degobert, "*Modeling and Thrust Control of PMLSM using Principle of Local Energy*," ICEMS2003, Beijing, P.R. China, 2003.
2. Thomas M. Jahns, Wen L. Soong, "*Pulsating Torque Minimization Techniques for Permanent Magnet AC Motor Drives – A Review*," IEEE Transactions on Industrial Electronics, Vol.43, No.2, April 1996, Pages.321-330.
3. P.L. Chapman, S.D. Sudhoff, C.A. Whitcomb, "*Optimal Control Strategies for Permanent-Magnet Synchronous Machine Drives*," IEEE Transactions on Energy Conversion, vol.14, No.4, pp.1043-1050, 1999.
4. J.Y. Hung, Z. Ding, "*Minimization of Torque Ripple in Permanent-Magnet Motors: A Closed Form Solution*," Proceedings of the 18th IEEE Industrial Electronics Conference, 1992, pp. 459-463.
5. T. Kosaka, N. Matsui, "*Optimal combination of pole configuration and current waveform of SRM for torque maximization*," Thirty-Third IAS Annual Meeting, the IEEE Industry Applications Conference, vol.1. Pages:586 - 592, 12-15 Oct. 1998.
6. Jun-Koo Kang, Seung-Ki Sul, "*New direct torque control of induction motor for minimum torque ripple and constant switching frequency*," Industry Applications, IEEE Transactions on , Volume: 35 , Issue: 5 , Sept.-Oct. 1999 Pages:1076 – 1082.
7. Lixin Tang, Limin Zhong, Muhammed Fazlur Rahman, Yuwen Hu, "*A Novel Direct Torque Control for Interior Permanent-Magnet Synchronous Machine Drive With Low Ripple in Torque and Flux – A Speed-Sensorless Approach*," IEEE Transactions on Industry Application, Vol.39, No.6, November/December 2003, pages. 1748-1756.
8. P.L. Chapman, S.D. Sudhoff, C.A. Whitcomb, "*Multiple Reference Frame Analysis of Non-sinusoidal Brushless DC Drives*," IEEE Transactions on Energy Conversion, Vol.14, No.3, September 1999.
9. P.L. Chapman, S.D. Sudhoff, "*Optimal control of permanent-magnet AC machine drives with a novel multiple reference frame estimator/regulator*," Thirty-Fourth IAS Annual Meeting. Conference Record of the 1999 IEEE Industry Applications Conference, Vol. 4, 3-7, Pages: 2567 – 2573, Oct. 1999.
10. Cheng-Tsung Liu, Sheng-Chuan Hsu, "*Analysis of linear electromagnetic motion devices by multiple-reference frame theory*," IEEE Transactions on Magnetics, Volume: 34, Issue: 4 , July 1998 Pages:2063 – 2065.
11. Jawad Faiz, B. Rezaei-Alam, "*Control of a linear Permanent Magnet Synchronous Motor using Multiple Reference Frame Theory*," Maglev'2002, pp.07-101, September 2002, Lausanne, Switzerland.
12. Y. Sato, T. Ishizuka, K. Nezu, T. Kataoka, "*A new control strategy for voltage-type PWM rectifiers to realize zero steady-state control error in input current*," IEEE Transactions on Industry Applications, Volume: 34 , Issue: 3 , May-June 1998 Pages: 480 – 486.

13. R.O. de Carvalho Jr, C.B. Jacobina, A.M.N. Lima, E.R.C. da Silva, "*Control of unbalanced three-phase power electronic systems*," Industry Applications Conference, 2000. Conference Record of the 2000 IEEE, Volume: 2, 8-12 Oct. 2000 Pages: 1317 - 1324 vol.2.

14. Xiaoming Yuan, W. Merk, H. Stemmler, J. Allmeling, "*Stationary-frame generalized integrators for current control of active power filters with zero steady-state error for current harmonics of concern under unbalanced and distorted operating conditions*," IEEE Transactions on Industry Applications, Volume: 38, Issue: 2, March-April 2002 Pages:523 – 532.

15. D.N. Zmood, D.G. Holmes, and G.H. Bode, "*Frequency-domain analysis of three-phase linear current regulators*," IEEE Trans. on Industrial Application., vol.37, pp.601-610, 2001.

16. D.N. Zmood, D.G. Holmes, "*Stationary frame current regulation of PWM inverters with zero steady-state error*," Power Electronics, IEEE Transactions on, Volume: 18, Issue: 3, May 2003 Pages: 814 – 822.

17. S. Fukuda, T. Yoda, "*A novel current-tracking method for active filters based on a sinusoidal internal model*," IEEE Transactions on Industry Applications, Volume: 37, Issue: 3, May-June 2001 Pages: 888 – 895.

18. J. Zeng, G. Remy, P.J. Barre, P. Degobert, "*Analysis of the influence of the initial pole position on the PMLSM thrust performances – Application to high speed machine tool*," Proceedings of the 4th International Symposium on Linear Drives for Industry Applications (LDIA2003), 8-10 September 2003, Birmingham, UK, Pages: 165-168.